

Article

High Cycle Fatigue Property of Carburized 20Cr Gear Steel under Axial Loading

Pengfei Liu, Wei Li *, Abdelhak Nehila, Zhenduo Sun and Hailong Deng

School of Mechanical Engineering, Beijing Institute of Technology, Beijing 100081, China; liu_perfect@126.com (P.L.); abdelhaknehila@hotmail.com (A.N.); bdsunzhenduo@126.com (Z.S.); deng_hl@126.com (H.D.)

* Correspondence: lliw@bit.edu.cn; Tel.: +86-10-6891-8730

Academic Editor: Hugo F. Lopez

Received: 31 March 2016; Accepted: 11 October 2016; Published: 18 October 2016

Abstract: The high cycle fatigue property of carburized 20Cr gear steel was experimentally investigated under axial loading with a stress ratio of zero. The test results show that this steel exhibits gradually decreasing *S-N* characteristics, and the fatigue strength corresponding to 10^9 cycles is about 455 MPa. Based on the observation of fracture surfaces, the interior inclusion fish-eye-induced fracture is the predominant fracture mode in the life regime beyond 10^5 cycles. The fine granular area (FGA) cannot be found clearly around the inclusion. Based on the evaluation of stress intensity factor ranges (ΔK) at the front of inclusion and fish-eye, the interior crack growth rate (da/dN) equation can be characterized by $da/dN = 2.39 \times 10^{-21}(\Delta K)^{12.32}$. Corresponding to the tested specimen, the predicted maximum inclusion size is about 52.02 μm . The predicted fatigue strength corresponding to 10^9 cycles by using Wang's model is slightly higher than the experimental result, but that by using Murakami's model is relatively conservative.

Keywords: high-strength steel; high cycle fatigue; interior-induced fracture; maximum inclusion size; fatigue strength

1. Introduction

In modern industries, more and more mechanical components or parts, such as gear, axle, and blade, etc., often have to be subjected to cyclic loading, and the actual load cycles greatly exceeds 10^7 cycles [1,2]. Moreover, it has been reported that these components or parts made of ferrous metals that are assumed to have a traditional fatigue limit at about 10^7 cycles can still fracture in the long life regime beyond 10^7 cycles [3–8]. Thus, it can be confirmed that the traditional fatigue design concepts are no longer satisfied with the demands of safety and reliability design for the mechanical components or parts in the long life regime. As an essential prerequisite, it is very necessary to clarify the fatigue properties of structural materials in the long life regime.

The change from surface-induced fracture to interior-induced fracture is the typical fracture feature of some high-strength steels in the long life regime [3,5–10]. Some metallurgical defects, such as non-metallic inclusions [3–8] or inhomogeneous microstructures [9,10] can play a very important role in causing the interior crack initiation. A propagating fish-eye-shaped crack can be observed on the fracture surface. Furthermore, a characteristic rough area indicating fine granular morphology—called “FGA” (fine granular area) by Sakai [11]—can sometimes occur around the defect. Thus, it can be concluded that the fatigue property of high-strength steel is greatly related to the characters of fish-eye, FGA, and inclusion, such as their sizes and positions. However, the relevant *S-N* properties and failure mechanisms are not yet well understood [4,8,12]. One of the major reasons is that the interior crack cannot be observed and measured during the experiment. Furthermore, from the viewpoint of safety design, the reliability of steel components in actual service can be affected by the maximum sizes of

defects contained in a certain bearing volume of steel [13–16]. How to reliably evaluate the maximum defect size, and then to predict the fatigue strength corresponding to a certain fatigue life, has been a key problem which researchers have to face.

In this study, the axial loading test of a carburized gear steel at a stress ratio of zero was performed to clarify the high cycle fatigue (HCF) property of this steel. According to the observation of fracture surfaces, the *S-N* property and failure mechanism were discussed. The stress intensity factor range at the front of a characteristic crack was evaluated, and the relevant interior crack growth rate equation was established. Combined with the prediction of maximum inclusion size, the fatigue strength at cycles of 10^9 of steel was predicted.

2. Materials and Methods

2.1. Material and Specimen

The investigated material in this study was a high-strength carburized 20Cr gear steel. Its main chemical composition (wt. %) is 0.18 C, 0.17 Si, 0.50 Mn, 0.03 S, 1.50 Cr, and 3.48 Ni. Specimens were first machined into hourglass shapes with a certain amount of finishing margin. Next, the heat treatment was carried out on the specimens. The heat treatment procedures were as follows: (a) carburizing process: carburized at $930\text{ }^{\circ}\text{C} \times 7\text{ h}$ + furnace cooling to $860\text{ }^{\circ}\text{C}$ + air cooling; (b) normalizing process: $840\text{ }^{\circ}\text{C} \times 0.5\text{ h}$ + air cooling; and (c) tempering process: $650\text{ }^{\circ}\text{C} \times 6\text{ h}$ + air cooling. After heat treatment, the microstructure of the steel is tempered martensite, and the depth of the carburized layer is about 1.2 mm. After etching with 4% alcohol nitric acid solution, the martensites with high carbon could be observed by scanning electron microscopy (SEM) in the carburized layer (shown in Figure 1a). In the core region, the martensites with low carbon could be observed by SEM (shown in Figure 1b). Finally, specimens were ground in a direction perpendicular to the axis of the specimen by grades 600–2000 abrasive paper to final shapes, as shown in Figure 2.

The minimum diameter and round notch radius of specimens are 6 mm and 47 mm, respectively. The Vickers hardness (HV) of the carburized layer and matrix region was measured by a nano-indenter G200, and its distribution as a function of the depth from the surface is presented in Figure 3. It can be found that first the value of HV on the surface is maximum, and then tends to decrease, finally approaching a constant of 455 at the depth exceeding about $1200\text{ }\mu\text{m}$. Therefore, it can be further confirmed that the thickness of the carburized layer is about $1200\text{ }\mu\text{m}$, and the value of HV for the matrix is about 455. In addition, the tensile strength of steel and the yield strength of 20Cr are 1483 MPa and 1292 MPa, respectively.

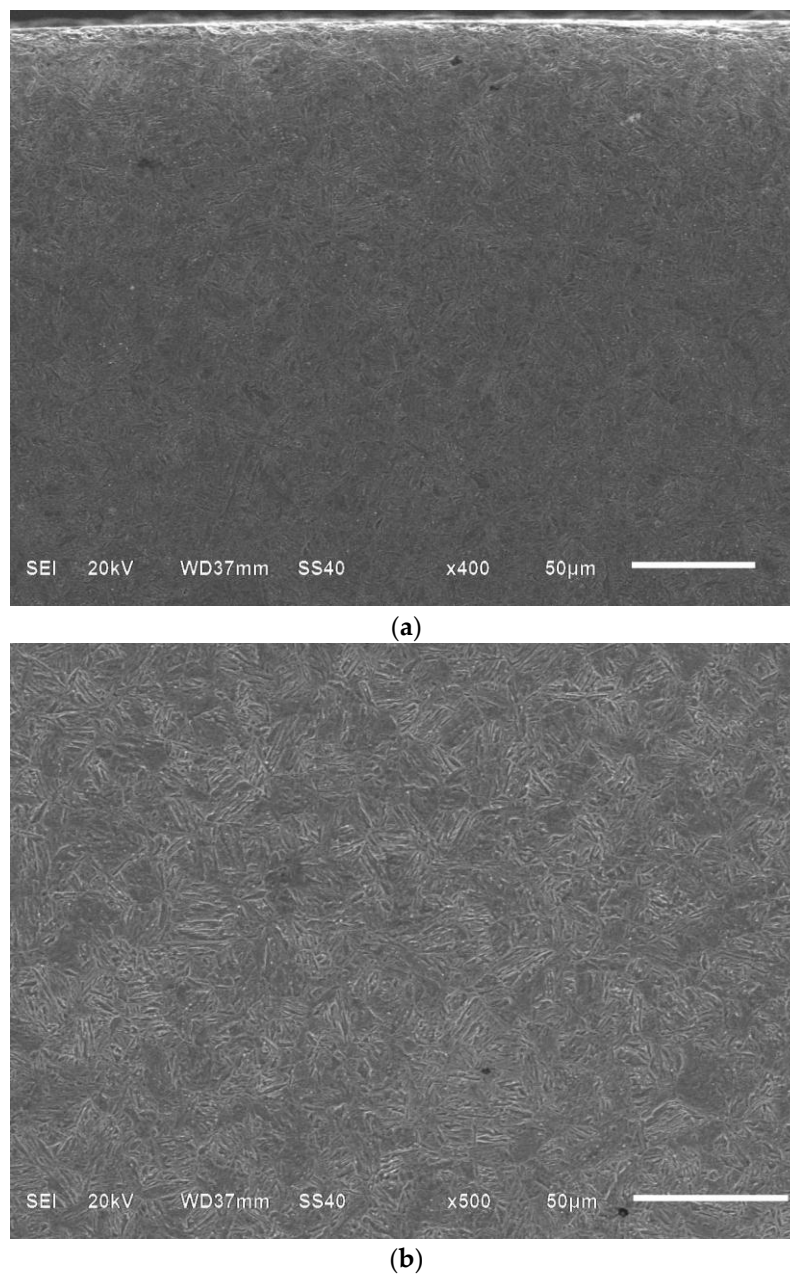


Figure 1. Observation of microstructure: (a) microstructure in carburized layer; (b) microstructure in core region.

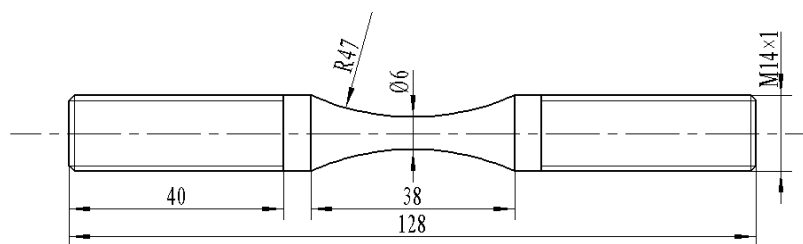


Figure 2. Shape and dimensions of specimen (units: mm).

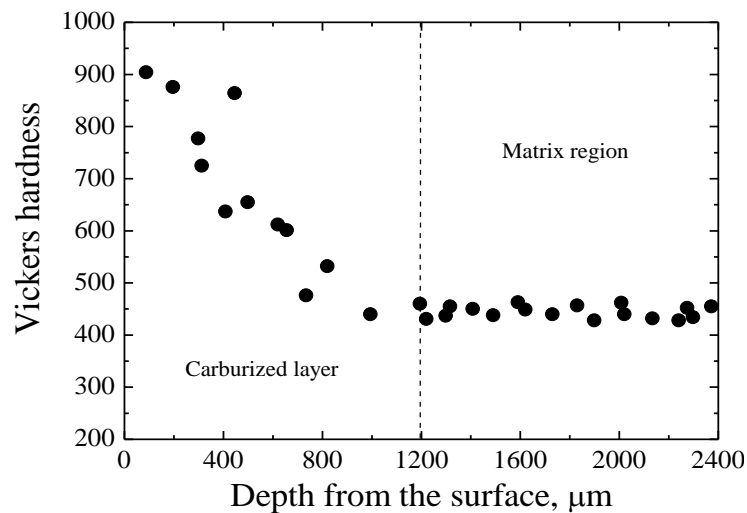


Figure 3. Vickers hardness of carburized layer and matrix region.

2.2. Testing Method

By using an electromagnetic resonant fatigue testing machine at a frequency of 100 Hz, the fatigue test of carburized 20Cr gear steel was carried out in an open environment and at room temperature with the constant stress ratio R of 0. After the experiment, fracture surfaces of all the failed specimens were carefully observed by scanning electron microscopy (SEM), especially paying attention to the crack initiation site and crack initiation and propagation mechanisms.

3. Results

3.1. S-N and P-S-N Characteristics

The S-N diagram of carburized 20Cr gear steel under axial loading with $R = 0$ is shown in Figure 4. There are two data points with fatigue lives exceeding 10^7 cycles. Furthermore, some maximum stress data exceed the yield strength slightly, but they do not have much influence on the experimental result. According to the SEM observation of all fracture surfaces, fatigue fractures of specimens can be divided into two modes: surface-induced fracture and interior-induced fracture. The surface-induced fracture occurs in the relatively high stress level with shorter fatigue life, whereas the interior-induced fracture occurs in the relatively low stress level with longer fatigue life. It can be confirmed that the interior-induced fracture is the predominant fracture mode of carburized 20Cr gear steel under axial loading in the life regime beyond 10^5 cycles. It should be noted that the so-called duplex S-N characteristics [3,7,11] cannot be distinctively observed. This can to some extent be attributed to the axial loading condition with the uniform stress distribution on the cross-section of the specimen. For the interior failure, it can be obviously seen that the relevant S-N property exhibits a continuously descending tendency, which is similar to the results of other steels with interior failure [1,3]. In view of the fact that the separation of test data corresponding to these two fracture modes is not so clear, a single S-N curve is plotted to represent the HCF characteristics of carburized 20Cr gear steel under axial loading with a stress ratio of zero, as shown in Figure 4. Consequently, based on the fitting S-N curve, the fatigue strength corresponding to the fatigue life of 10^9 cycles, σ_f , is evaluated to be about 455 MPa.

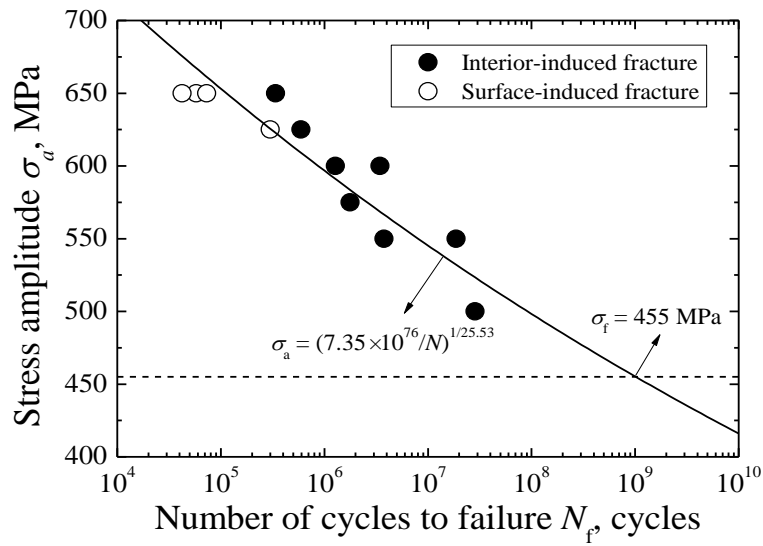


Figure 4. S-N diagram of carburized 20Cr steel under axial loading with $R = 0$.

According to the JSMS-SD-6-04 [17], the error in the regression model is generally expressed in normal distribution of $N(0, s^2)$ where s^2 is the error variance used in regression analysis. This means a model with constant variance in the error distribution showing residuals. That is, for any value of the explanatory variances, the error distribution of the objective variable in the applied model conforms to the normal distribution, with constant variance expressed in $N(0, s^2)$. Therefore, in consideration of the fact that the peculiar scatter of σ_a -value can be better characterized by the normal distribution, the σ_a -value can be taken as the objective variable, while the value of N can be taken as the explanatory variable. Combined with the S-N equation, the P-S-N curve of carburized 20Cr gear steel can be expressed as:

$$\sigma_a = \left(\frac{7.35 \times 10^{76}}{N} \right)^{\frac{1}{25.53}} - \mu_p \cdot s \tag{1}$$

where s denotes the standard deviation in σ_a -value distribution, and μ_p is the standard normal variate corresponding to a given probability. In fact, the value of σ_a obtained from the S-N equation is just the value of σ_a under $P = 50\%$. Thus, the values of σ_a at five survival probabilities, including 1%, 10%, 50%, 90%, and 99%, can be calculated, and the relevant P-S-N curves are plotted in Figure 5.

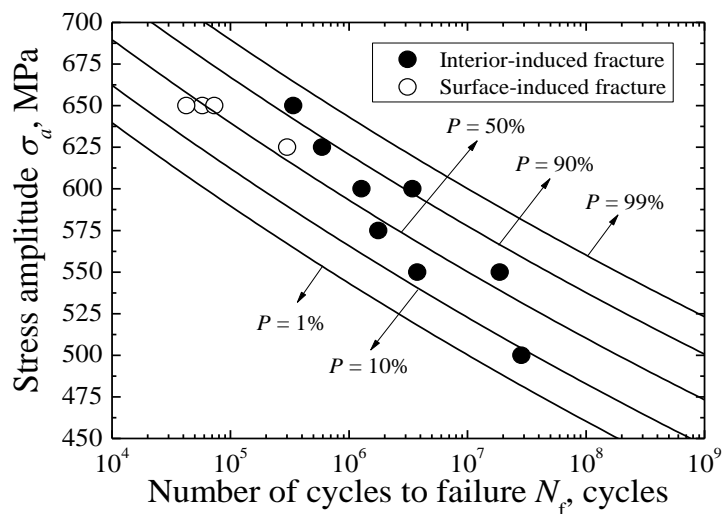


Figure 5. P-S-N diagram of carburized 20Cr steel under axial loading with $R = 0$.

3.2. Crack Initiation Mode

As previously mentioned, fatigue fractures of specimens consist of surface-induced fracture and interior-induced fracture. For the surface-induced fracture, fatigue cracks all originate from machining defects, as shown in Figure 6a.

For interior-induced fracture, the nonmetallic inclusion plays a key role in causing the crack initiation. An isolated fisheye can be found on the fracture surface, and the inclusion is basically located at the center of the fisheye, as shown in Figure 6b. However, the FGA cannot be observed around the inclusion whether the fatigue life is beyond 10^7 cycles (Figure 6b,c) or the fatigue life is below 10^7 cycles (Figure 6d,e). Obviously, the interior crack initiation is the predominant failure mode of this carburized steel. First, it is attributed to the existence of surface compressive residual stress and surface harder layer caused by carburization. Furthermore, in order to keep the mechanical state of equilibrium, the slight tensile residual stress can also exist in the interior matrix region, especially approaching the carburized layer. Therefore, it can also promote the interior crack initiation to some extent.

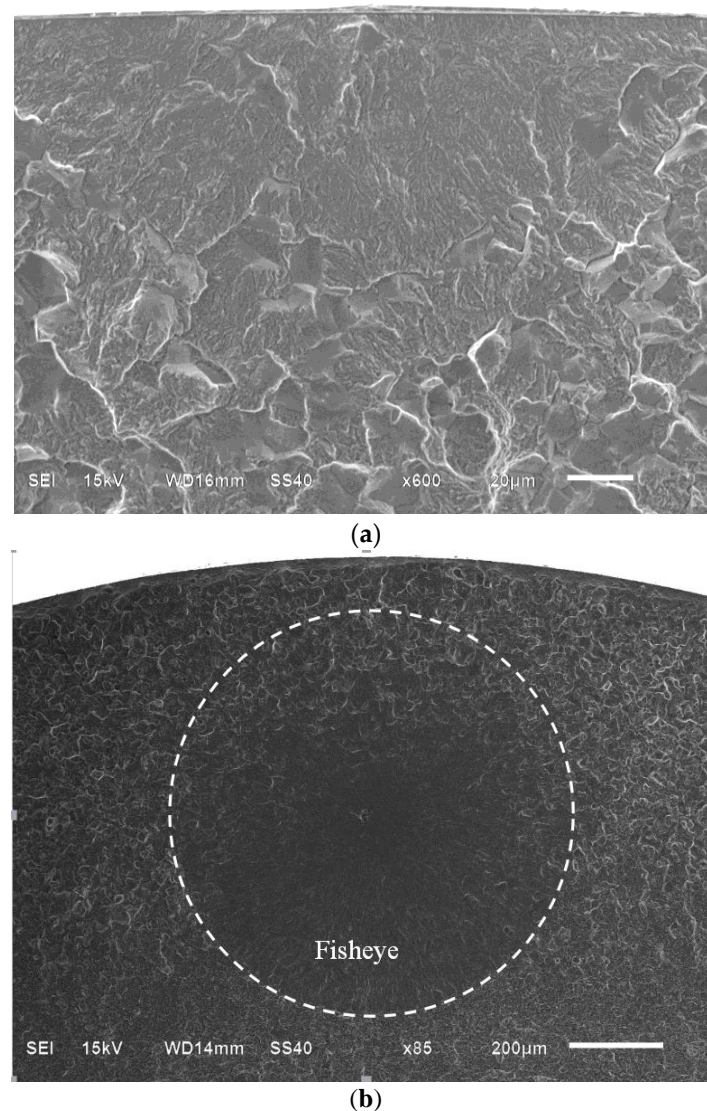


Figure 6. Cont.

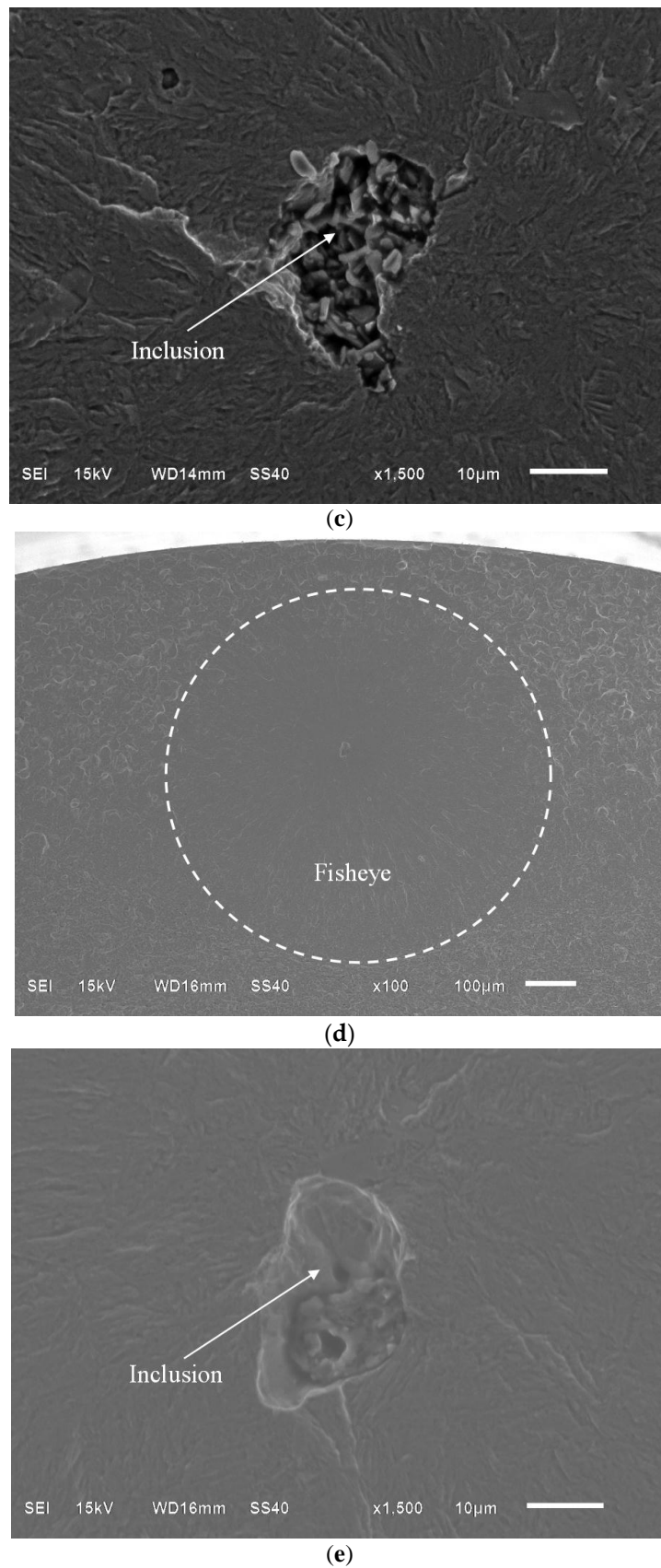


Figure 6. SEM observation of fracture surfaces: (a) Surface defect-induced fracture ($\sigma_a = 625$ MPa, $N_f = 300,600$); (b) Fisheye in the high cycle fatigue (HCF) regime beyond 10^7 cycles ($\sigma_a = 550$ MPa, $N_f = 18,704,700$); (c) Inclusion without fine granular area (FGA, $\sigma_a = 550$ MPa, $N_f = 18,704,700$); (d) Fisheye in HCF regime below 10^7 cycles ($\sigma_a = 550$ MPa, $N_f = 3,765,500$); (e) Inclusion without FGA ($\sigma_a = 550$ MPa, $N_f = 3,765,500$).

3.3. Characteristic Crack Size

Based on the fractography, several parameters were defined to discuss interior defect/crack geometrical characteristics. The parameter d_{inc} denotes the depth of inclusion from its center to the nearest fracture surface edge. Furthermore, the parameter $(area)^{1/2}$ denotes the size of the defect or crack, evaluated by the square root of its area. For the inclusion and the fisheye, their sizes are indicated by $(area_{inc})^{1/2}$ and $(area_{fisheye})^{1/2}$ (including $(area_{inc})^{1/2}$), respectively.

Figure 7 shows the relationship between d_{inc} and N_f . Most of the values of d_{inc} are in the range of 13,546–24,338 μm , and are larger than the thickness of carburized layer, whereas only two values of d_{inc} are less than it. This means that the carburized layer can effectively restrain the possibility of fatigue crack initiation originating from inclusions contained in the layer itself. Furthermore, it can be seen that the values of d_{inc} are almost regardless of fatigue life.

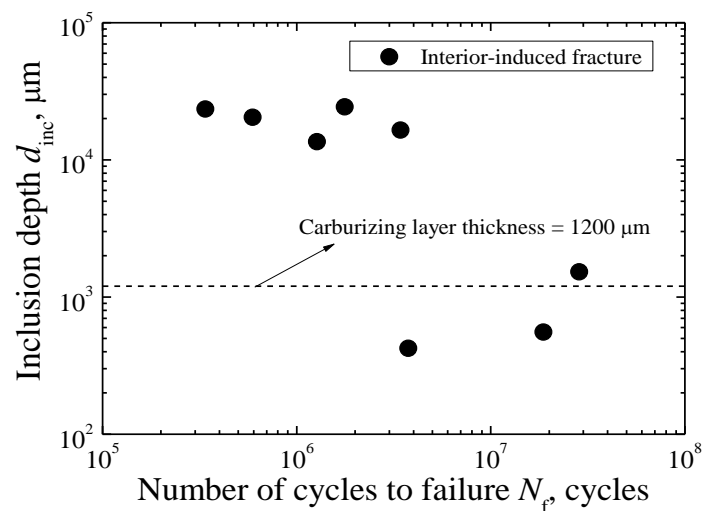


Figure 7. Relationship between d_{inc} and N_f .

The Figure 8 shows the relationships between $(area_{inc})^{1/2}$ and $(area_{fisheye})^{1/2}$, and σ_a . The values of $(area_{inc})^{1/2}$ are scattered in the range of 17.1–36.3 μm with an average value of 26.8 μm , while the values of $(area_{fisheye})^{1/2}$ are scattered in the range of 643.5–1664.1 μm with an average value of 900.1 μm .

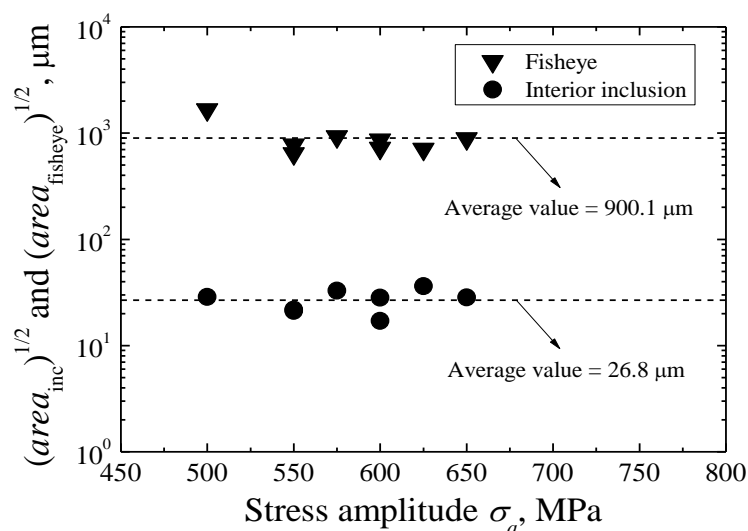


Figure 8. Relationship between $(area_{inc})^{1/2}$ and $(area_{fisheye})^{1/2}$, and σ_a .

4. Discussion

4.1. Evaluation of Interior Crack Growth Rate

The interior inclusions can be regarded as pre-existing cracks [13], and the shapes of the inclusion and fisheye are approximately circular. Thus, the stress intensity factor range ΔK at the front of the inclusion and fisheye, ΔK_{inc} and $\Delta K_{\text{fisheye}}$, can be given by [18]:

$$\Delta K = \frac{2}{\pi} \Delta \sigma \sqrt{\pi r} = \frac{2}{\pi} \Delta \sigma \sqrt{\sqrt{\pi a \text{area}}} \quad (2)$$

where r denotes the radius of the defect or crack, and $\Delta \sigma$ is the applied stress range.

Based on the theory of linear elastic fracture mechanics, the test data with the stress amplitude of 650 MPa is not considered in the following calculation. Figure 9 shows the relationship between ΔK_{inc} and N_f . The values of ΔK_{inc} are in the range of 4.39–6.67 MPam^{1/2}, and tend to decrease with the increase of fatigue life. It should be noted that the values of ΔK_{inc} are similar to or slightly larger than the values of stress intensity factor range at the front of the FGA, ΔK_{FGA} , reported for some high-strength steel [19]. This is the reason why the FGA cannot be observed in the vicinity of the inclusion. In other words, the inclusion size is large enough and exceeds the critical size corresponding to ΔK_{FGA} , and fatigue crack can directly enter into the stable crack propagation stage under cyclic loading; i.e., the formation period of a fisheye outside of inclusion. Figure 10 shows the relationship between $\Delta K_{\text{fisheye}}$ and N_f . The values of $\Delta K_{\text{fisheye}}$ are in the range of 23.66–34.59 MPam^{1/2}, with an average value of 28.50 MPam^{1/2}, which are very similar to the fatigue fracture toughness of this steel. Thus, it can be assumed that $\Delta K_{\text{fisheye}}$ is the threshold value controlling the unstable growth of interior cracks.

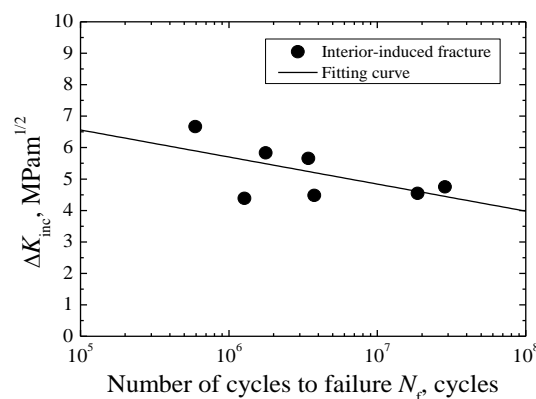


Figure 9. Relationship between ΔK_{inc} and N_f .

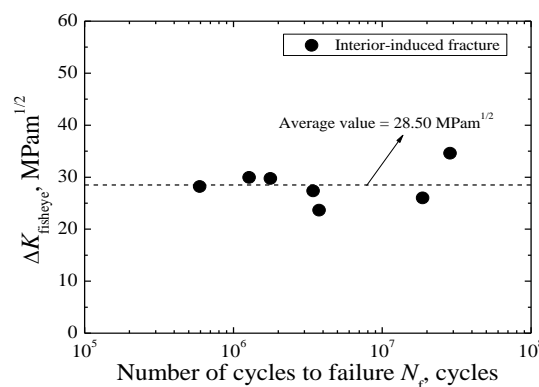


Figure 10. Relationship between $\Delta K_{\text{fisheye}}$ and N_f .

Based on Tanaka’s theory [20], the interior crack growth rate from the inclusion to the fisheye, da/dN , can be described by the Paris law:

$$da/dN = C(\Delta K)^m \tag{3}$$

where C and m are material constants. Studies have shown that the majority of the total fatigue life is consumed in the stage of fisheye formation [21], so the value of N can be regarded approximately as the total fatigue life N_f . Combined with Equation (2), Equation (3) can be rewritten as:

$$(\Delta K_{inc})^m (N/area_{inc}^{1/2}) = [2/C(m-2)] [1 - (\sqrt{area_{inc}/area_{fisheye}})^{\frac{m}{2}-1}] \tag{4}$$

The relationship between ΔK_{inc} and $N/area_{inc}^{1/2}$ is shown in Figure 11. Combined with the evaluated sizes of inclusion and fisheye, as well as the S-N data, the values of C and m can be obtained. Thus, the interior crack growth rate equation from the inclusion to the fisheye can be expressed as:

$$da/dN = 1.05 \times 10^{-20} (\Delta K)^{11.45} \tag{5}$$

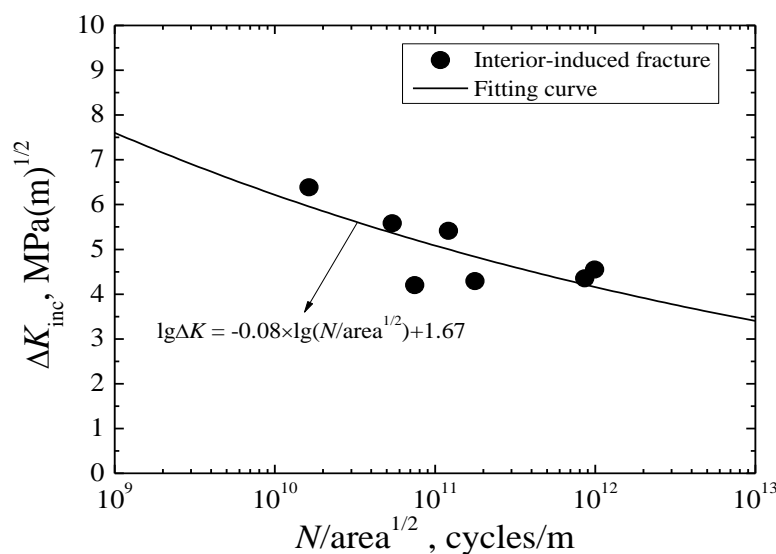


Figure 11. Relationship between ΔK_{inc} and $N/area^{1/2}$.

4.2. Prediction of Maximum Inclusion Size

Based on the statistics of extreme values (SEV) presented by Murakami et al. [22], the maximum inclusion size in a given control volume of steel, V (units: mm^3), can be predicted. Firstly, it is confirmed that the measured sizes of inclusions observed on the fracture surfaces can be well characterized by the Gumbel distribution, and the corresponding cumulative distribution function $F(x)$ is given by:

$$F(x) = \exp \{ -\exp \{ -[(x - \lambda)/\alpha] \} \} \tag{6}$$

where λ and α are location parameter and scale parameter, respectively. The size of the i th inclusion, x_i , are classified, starting from the smallest and indexed with $i = 1, 2, \dots, J$, where J denotes the number of inclusions. For small samples, the cumulative probability corresponding to x_i is expressed as:

$$P(x_i) = (i - 0.3)/(J + 0.4) \tag{7}$$

Based on Equations (6) and (7), the following equations can be obtained as:

$$y_i = (x_i - \lambda)/\alpha \tag{8}$$

$$y_i = -\ln \{ -\ln [(i - 3)/(J + 0.4)] \} \tag{9}$$

Thus, a straight line with slope α and intercept λ indicating relationship between x_i and y_i can be plotted in Figure 12. The fitted values of λ and α are 23.9 and 5.65, respectively. Let X_V denote the characteristic value of maximum inclusion size in units of μm , the return period, T , and the cumulative probability of X_V , $P(X_V)$, are given by:

$$T = V/V_0 \quad (10)$$

$$P(X_V) = 1 - 1/T \quad (11)$$

where V_0 is the volume of a standard inspection plane, S_0 , with a certain thickness. Under axial loading, S_0 is the area of the minimum cross-section of the specimen (about 28.26 mm^2), and its thickness value is approximately defined as the mean size of inclusions (about $26.8 \mu\text{m}$). Thus, the value of V_0 is evaluated to be about 0.76 mm^3 . Therefore, the value of X_V can be evaluated by the following equation:

$$X_V = 23.9 - 5.65 \ln[-\ln(1 - 0.76/V)] \quad (12)$$

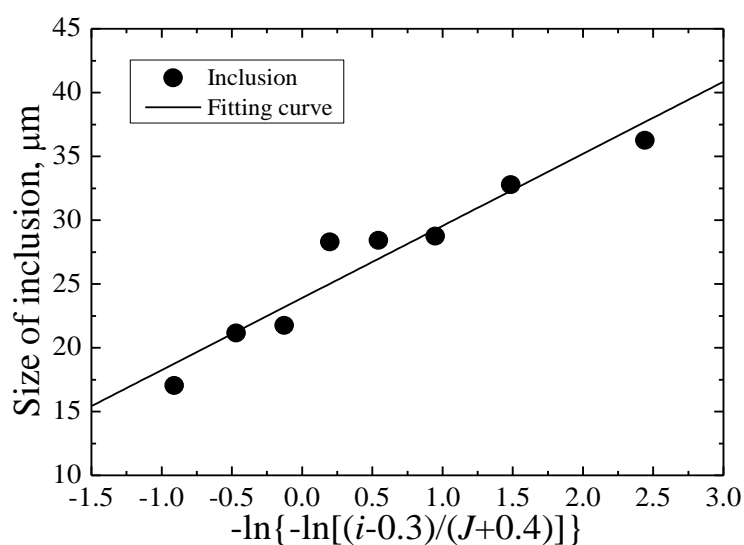


Figure 12. Fitted values of Gumbel distribution parameter α and λ .

Figure 13 shows the predicted maximum inclusion sizes as a function of V for carburized 20Cr steel. They tend to increase with the increase of V . For the specimen tested in this study, the tested volume V can be expressed as [22]:

$$V = 0.25\pi l d^2 \quad (13)$$

where d is the diameter of minimum cross-section, l is defined as the length at which the stress value on the cross-section is 0.9 times that on minimum cross-section at $l/2$. Herein, the values of d and l are 6 mm and 3.9 mm, respectively. Thus, the value of V is 110.28 mm^3 , and the relevant maximum inclusion size is about $52.02 \mu\text{m}$.

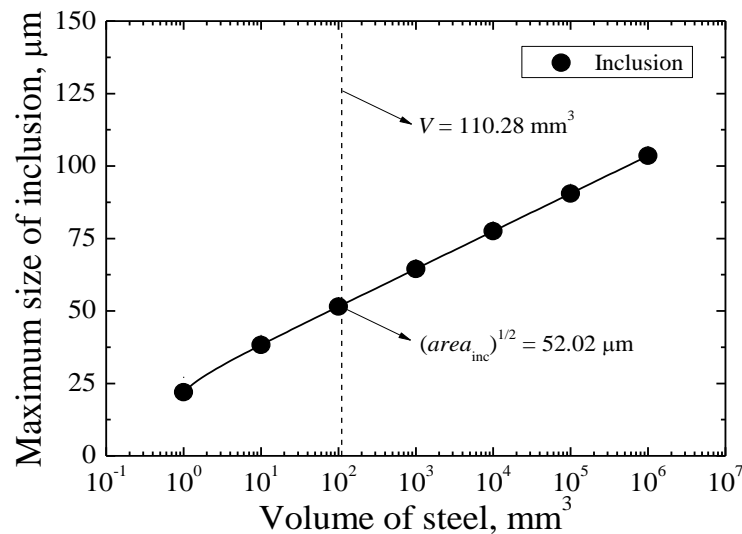


Figure 13. Prediction of maximum inclusion size.

4.3. Prediction of the Fatigue Strength at 10^9 Cycles

A theoretical model proposed by Murakami can be used to predict the fatigue strength at 10^9 cycles, σ_w , corresponding to the interior inclusion-induced fracture under a certain stress ratio, and is given by [23]:

$$\sigma_w = [1.56(\text{HV} + 120) / (\text{area}^{1/2})^{1/6}] [(1 - R) / 2]^\beta \quad (14)$$

where $\beta = 0.226 + \text{HV} \times 10^{-4}$. The value of HV for carburized 20Cr steel is 455, so the value of β is evaluated to be 0.2715. For surface inclusion, the value of area parameter $\text{area}^{1/2}$ must be less than 1000 μm . For interior inclusion, the value of $\text{area}^{1/2}$ does not have this limit [24]. All inclusions are interior in this study. Furthermore, considering the effect of fatigue life, Wang modified this model and presented a new model, as follows [5]:

$$\sigma_w = [\gamma(\text{HV} + 120) / (\text{area}^{1/2})^{1/6}] [(1 - R) / 2]^\beta \quad (15)$$

where $\gamma = 3.09 - 0.12 \log N_f$ for the interior inclusion-induced fracture. Herein, the value of N_f is defined to be 10^9 cycles. Based on these two models, Figure 14 shows the predicted values of σ_w as a function of steel volume for carburized 20Cr steel under axial loading.

It can be seen from Figure 14 that the predicted values of the fatigue strength at 10^9 cycles tend to decrease with the increase of steel volume, which is in inverse proportion to the predicted results of maximum inclusion size. For the tested volume of a specimen with about 110.28 mm^3 , the predicted results by using Murakami's model and Wang's model are 385 MPa and 496 MPa, respectively. Compared with the experimental result of about 455 MPa corresponding to 10^9 cycles, the predicted result based on Wang's model is a little higher, whereas that based on Murakami's model is relatively low but is safe.

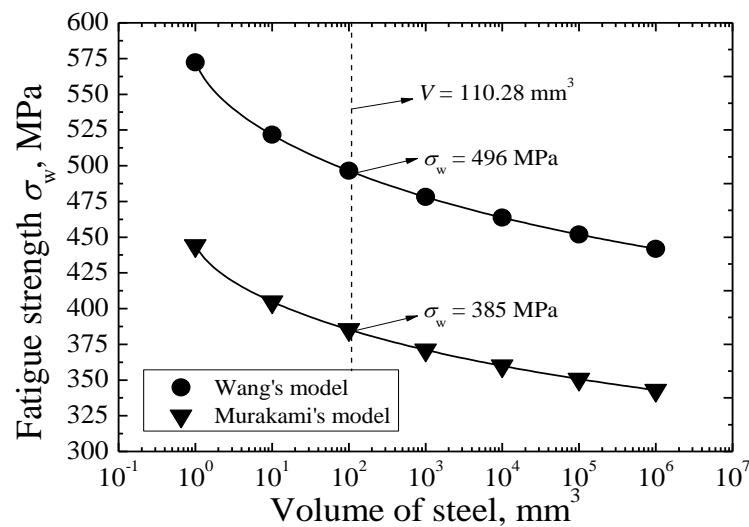


Figure 14. Prediction of the fatigue strength at 10^9 cycles.

5. Conclusions

In this study, main conclusions obtained are listed as follows:

1. The carburized 20Cr gear steel shows continuously decreasing $S-N$ characteristics without a traditional fatigue limit, and the fatigue strength corresponding to 10^9 cycles is about 455 MPa.
2. The interior inclusion-fisheye-induced fracture is main fracture mode in the HCF regime, but the FGA cannot be found in the vicinity of the inclusion.
3. Based on the evaluation of stress intensity factor ranges at the front of inclusion and fisheye, the interior crack growth rate equation from the inclusion to fisheye can be established; i.e., $da/dN = 2.39 \times 10^{-21}(\Delta K)^{12.32}$.
4. Based on the SEV method, the predicted maximum inclusion size is about 52.02 μm and is larger than the observed inclusion size.
5. The predicted fatigue strength corresponding to 10^9 cycles by using Wang's model is slightly higher than the experimental result, but that by using Murakami's model is relatively conservative.

Acknowledgments: This research was supported by the National Natural Science Foundation of China (No. 51305027).

Author Contributions: Wei Li conceived and designed the experiment; Pengfei Liu and Abdelhak Nehila performed the experiments; Zhenduo Sun and Hailong Deng observed the fracture surfaces; Pengfei Liu and Nehila Abdelhak analyzed and processed the data; Pengfei Liu and Wei Li wrote the paper.

Conflicts of Interest: The authors declare no conflict of interest.

References

1. Bathias, C. There is no infinite fatigue life in metallic materials. *Fatigue Fract. Eng. Mater. Struct.* **1999**, *22*, 559–565. [[CrossRef](#)]
2. Bandara, C.S.; Siriwardane, S.C.; Dissanayake, U.I.; Dissanayake, R. Fatigue failure predictions for steels in the very high cycle region—A review and recommendations. *Eng. Fail. Anal.* **2014**, *45*, 421–435. [[CrossRef](#)]
3. Li, W.; Sakai, T.; Li, Q.; Lu, L.T.; Wang, P. Reliability evaluation on very high cycle fatigue property of GCr15 bearing steel. *Int. J. Fatigue* **2010**, *32*, 1096–1107. [[CrossRef](#)]
4. Deng, H.L.; Li, W.; Sakai, T.; Sun, Z.D. Very high cycle fatigue failure analysis and life prediction of Cr-Ni-W gear steel based on crack initiation and growth behaviors. *Materials* **2015**, *8*, 8338–8354. [[CrossRef](#)]
5. Wang, Q.Y.; Berard, J.Y.; Dubarre, A.; Baudry, G.; Rathery, S.; Bathias, C. Gigacycle fatigue of ferrous alloys. *Fatigue Fract. Eng. Mater. Struct.* **1999**, *22*, 667–672. [[CrossRef](#)]

6. Sohar, C.R.; Betzwar-Kotas, A.; Gierl, C.; Weiss, B.; Danninger, H. Gigacycle fatigue behavior of a high chromium alloyed cold work tool steel. *Int. J. Fatigue* **2008**, *30*, 1137–1149. [[CrossRef](#)]
7. Li, W.; Sakai, T.; Li, Q.; Lu, L.T.; Wang, P. Effect of loading type on fatigue properties of high strength bearing steel in very high cycle regime. *Mater. Sci. Eng. A* **2011**, *528*, 5044–5052. [[CrossRef](#)]
8. Li, W.; Sun, Z.D.; Zhang, Z.Y.; Deng, H.D.; Sakai, T. Influence of case-carburizing and micro-defect on competing failure behaviors of Ni-Cr-W steel under gigacycle fatigue. *Int. J. Fatigue* **2015**, *72*, 66–74. [[CrossRef](#)]
9. Yu, Y.; Gu, J.L.; Xua, L.; Shou, F.L.; Bai, B.Z.; Liu, Y.B. Very high cycle fatigue behaviors of Mn-Si-Cr series bainite/martensite dual phase steels. *Mater. Des.* **2010**, *31*, 3067–3072. [[CrossRef](#)]
10. Yu, Y.; Gu, J.L.; Bai, B.Z.; Liu, Y.B.; Li, S.X. Very high cycle fatigue mechanism of carbide-free bainite/martensite steel micro-alloyed with Nb. *Mater. Sci. Eng.* **2009**, *527*, 212–217. [[CrossRef](#)]
11. Sakai, T.; Takeda, M.; Shiozawa, K.; Ochi, Y.; Nakajima, M.; Nakamura, T. Experimental reconfirmation of characteristic *S-N* property for high carbon chromium bearing steel in wide life region in rotating bending. *J. Soc. Mater. Sci. Jpn.* **2000**, *49*, 779–785. [[CrossRef](#)]
12. Lai, J.; Lund, T.; Ryden, K.; Gabelli, A.; Strandell, I. The fatigue limit of bearing steels—Part 1: A pragmatic approach to predict very high cycle fatigue strength. *Int. J. Fatigue* **2012**, *37*, 155–168. [[CrossRef](#)]
13. Murakami, Y.; Nomoto, T.; Ueda, T.; Ohtori, M. Analysis of the mechanism of superlong fatigue failure by optical microscope and SEM/AFM observations. *J. Soc. Mater. Sci. Jpn.* **1999**, *48*, 1112–1117. [[CrossRef](#)]
14. Yang, Z.G.; Zhang, J.M.; Li, S.X.; Li, G.Y.; Wang, Q.Y.; Hui, W.J. On the critical inclusion size of high strength steels under ultra-high cycle fatigue. *Mater. Sci. Eng. A* **2006**, *427*, 167–174. [[CrossRef](#)]
15. Zhang, J.M.; Zhang, J.F.; Yang, Z.G.; Li, G.Y.; Yao, G.; Li, S.X.; Hui, W.J.; Weng, Y.Q. Estimation of maximum inclusion size and fatigue strength in high-strength ADF1 steel. *Mater. Sci. Eng. A* **2005**, *394*, 126–131. [[CrossRef](#)]
16. Mayer, H.; Papakyriacou, M.; Zettl, B.; Vacic, S. Endurance limit and threshold stress intensity of die cast magnesium and aluminium alloys at elevated temperature. *Int. J. Fatigue* **2005**, *27*, 1076–1088. [[CrossRef](#)]
17. JSMS-SD-6-04. *Standard Evaluation Method of Fatigue Reliability for Metallic Materials-Standard Regression Method of S-N Curves*; The Society of Material Science: Tokyo, Japan, 2004.
18. Israel, M.G.; Paul, C.P.; Hiroshi, T.; Claude, B. Fatigue crack growth from small to long cracks in very-high-cycle fatigue with surface and internal “fish-eye” failures for ferrite-perlitic low carbon steel SAE 8620. *Mater. Sci. Eng. A* **2007**, *468–470*, 120–128.
19. Sakai, T.; Sato, Y.; Oguma, N. Characteristic *S-N* properties of high-carbon-chromium-bearing steel under axial loading in long-life fatigue. *Fatigue Fract. Eng. Mater. Struct.* **2002**, *25*, 765–773. [[CrossRef](#)]
20. Tanaka, K.; Akiniwa, Y. Fatigue crack propagation behavior derived from *S-N* data in very high cycle regime. *Fatigue Fract. Eng. Mater. Struct.* **2002**, *25*, 775–784. [[CrossRef](#)]
21. Sun, Z.D.; Li, W.; Deng, H.L.; Zhang, Z.Y. Fish-eye failure analysis and life design approach for case-carburized gear steel based on statistical evaluation of defect size. *Eng. Fail. Anal.* **2016**, *59*, 28–40. [[CrossRef](#)]
22. Murakami, Y.; Chen, D.; Nisitan, H.; Mori, K. *Stress Intensity Factor Handbook*, 3rd ed.; Society of Materials Science-Pergamon: Tokyo, Japan, 1993; pp. 661–662.
23. Murakami, Y.; Endo, M. Effect of hardness and crack geometry on delta K threshold of small cracks. *J. Soc. Mater. Sci. Jpn.* **1985**, *35*, 911–917. [[CrossRef](#)]
24. Murakami, Y. Quantitative Evaluation of Effects of Defects and Defects and Non-metallic Inclusions on Fatigue Strength of Metal. *Tetsu-to-Hagane* **1989**, *75*, 1267–1277.

